International Journal of Engineering

Radar Absorption Performance of Fe₃O₄/AC/PANI Nanocomposites Prepared from Natural Iron Sand

A. Taufiq*[a], R. Sutiami[a], S. U. I. Subadra[a], A. Hidayat[a], M. Diantoro[a], S. Sunaryono[a], N. Hidayat[a], W. A. Adi[b]

[a] Department of Physics, Faculty of Mathematics and Natural Sciences, Universitas Negeri Malang, Indonesia
[b] Centre for Technology of Nuclear Industry Materials, National Nuclear Energy Agency, Tangerang, Indonesia

P A P E R   I N F O

A B S T R A C T

In this work, the Fe_3O_4 nanoparticles from natural iron sand were combined with active carbon (AC) and polyaniline (PANI) to obtain Fe_3O_4/AC/PANI nanocomposites with mass variations of the AC of 0.1, 0.2, 0.3, 0.4, and 0.5 g. The crystalline phase of Fe_3O_4/AC/PANI nanocomposites formed from Fe_3O_4 with PANI having an amorphous phase. Meanwhile, the crystalline phase of AC was unmatched because of its very small composition. The presence of AC was observed through vibrations from the C-C and COOH functional groups. The existence of PANI was indicated by the vibrations of the benzoic ring and quinonoid bonds. Besides, the presence of Fe_3O_4 was confirmed by the presence of Fe-O functional groups from octahedral and tetrahedral positions. The optical properties of Fe_3O_4/AC/PANI nanocomposites were shown by increasing the energy gap along with decreasing absorption wavelength. Interestingly, increasing AC composition made the absorption bandwidth of the Fe_3O_4/AC/PANI nanocomposites wider, so that the radar absorption also increased marking by the greater reflection loss that reached -15.8 dB. The increase in the radar absorption performance of Fe_3O_4/AC/PANI nanocomposites came from the efficient complementarity between dielectric loss and magnetic loss and interfacial polarization between Fe_3O_4-AC or between Fe_3O_4-PANI.

doi: 10.5829/ije.2020.33.02b.15

NOMENCLATURE

RAM	Radar Absorbing Material	XRD	X-ray Diffraction
RL	Reflection Loss	IR	InfraRed
PANI	polyaniline	SEM	Scanning Electron Microscopy
AC	Activated Carbon		

1. INTRODUCTION

In the last decades, the applications of electromagnetic wave-based equipment in various fields have been expanded rapidly. On the other hand, the use of electromagnetic waves can also cause problems in environmental pollution, human health, electromagnetic interference, and so forth [1]. Consequently, to unravel this problem, studies related to the design and fabrication of electromagnetic wave absorbers become essential to be conducted.

One of the studies on electromagnetic wave absorbers which began to be widely studied by researchers was radar absorbing materials (RAM) [2,3]. Theoretically, RAM is an absorbent material for microwaves that works by reducing the radar cross-section or converting microwaves to heat energy [4]. It thus alleviates the reflection (*RL*) of the radar so that the pollution caused can be reduced. In addition, one of the resilient reasons why research related to RAM began to develop rapidly is because RAM can be applied to the military field to assist the defense of a country in terms of protection strategies during the war [5]. Technically, RAM coating on a fighter or warship decreases the cross-section of the radar [6], so that the reflected waves decrease or even disappear.

Corresponding Author Email: ahmad.taufiq.fmipa@um.ac.id (A. Taufiq)

In general, radar waves consist of magnetic and dielectric components in perpendicular directions [7]. Therefore, the development of RAM fabrication is worthdoing through engineering composite materials that have excellent magnetic and dielectric properties to maximize radar absorption [8]. One magnetic material that is incredibly promising for RAM is Fe_3O_4 nanoparticles inasmuch it possesses high magnetization and permeability characteristics [9], good flexibility [10], excellent chemical and thermal stability [11]. Unfortunately, Fe_3O_4 entails disadvantages since it has low dielectric properties, easily agglomerated [12], and high density which affects the absorption of radar waves [3]. On the other hand, RAM applications require materials that have a wide bandwidth [13] with low density [14]. Therefore, Fe_3O_4 nanoparticles need to be modified with other materials that have dielectric properties and low density, such as with polyaniline polymers (PANI).

Based on previous works, it was observed that PANI is a polymer which has a high conductivity [1], controlled dielectricity, good environmental stability [15], high conductivity, and low density [16]. Thus, this material has extremely decent potential as RAM that is compiled with Fe_3O_4 nanoparticles. With regard to this fact, a previous study has also succeeded in synthesizing RAM based on Fe_3O_4/PANI composites with reflection loss (*RL*) values of less than -10 dB [17]. However, for special applications that require high absorption, to refine the performance of the Fe_3O_4/PANI composites in radarabsorbing is needed. Therefore, to refine its absorption performance, the Fe_3O_4 PANI composites need to be modified by adding other materials that have a wide surface and porous structure in forming more complex nanocomposites.

Based on previous studies, it is observed that activated carbon (AC) is a dielectric material that has a high absorption [18–20] since it has a large surface area and a porous structure [21]. Other research also proved that the AC/Fe_3O_4 composites application employed as a microwave absorbing material successfully obtained a maximum *RL* of -10.09 dB [22]. Therefore, through the development of new fabrication materials based on the combination of Fe_3O_4, PANI, and AC to form the nanocomposites Fe_3O_4/AC/PANI proposed in this work is potential to advance the performance of radar absorption far better than before. The hypothesis that there is an increase in the performance of radar absorption through the importance of the nanocomposites application is at least predictable due to the effect of efficient complementarity between dielectric loss and magnetic loss and interfacial polarization between Fe_3O_4 and AC or between Fe_3O_4 and PANI.

While it is insufficient to modify the Fe_3O_4/AC/PANI nanocomposites to increase its absorption of radar waves, the development of inexpensive and simple synthesis methods to reduce fabrication costs are encouraged. Thereby, in this work, we developed natural fabrication methods of Fe_3O_4/AC/PANI nanocomposites in the form of iron sand using a simple precipitation method. Iron sand that is easily obtained in abundant quantities in almost all regions of Indonesia provides new opportunities in the fabrication of inexpensive and environmentally friendly Fe_3O_4/AC/PANI nanocomposites. While choosing the precipitation method can only be done at room temperature, the process is simple, fast, and low-cost. Furthermore, to find out the optimal performance of nanocomposite absorption, in this work, the effect of AC composition variation on the absorption of Fe_3O_4/AC/PANI nanocomposites radar waves is examined. The different weight ratios of AC: (Fe_3O_4/AC/PANI) nanocomposites were of 1:30, 2:30, 3:30, 4:30, and 5:30. Nonetheless, the study of the structure, functional groups, morphology and particle size, and the optical properties of Fe_3O_4/AC/PANI are also an important part of this work.

2. MATERIALS AND METHODS

2. 1. Materials   The materials used in this work are Indonesian iron sand, HCl, NH_4OH, H_2O, $C_6H_5NH_2$, $(NH)_4S_2O_8$, and AC.

2. 2. Synthesis of Fe_3O_4/AC Nanocomposites In this work, the Fe_3O_4/AC nanocomposites were fabricated using the coprecipitation method started with the preparation of $FeCl_2$ and $FeCl_3$ solutions through the reaction of the iron sand with HCl. A total of 15 ml of $FeCl_2$ and $FeCl_3$ solutions added by AC with composition variations of 0.1, 0.2, 0.3, 0.4, and 0.5 g were employed. Subsequently, the solution was stirred for 35 minutes and followed by the NH_4OH titration process to obtain concentrated black deposits which were Fe_3O_4/AC deposits. Furthermore, the precipitate was washed by using H_2O to obtain a pH = 7 and dried at 100 °C to obtain Fe_3O_4/AC nanocomposites.

2. 3. Synthesis of PANI   PANI powder was synthesized by using the in-situ polymerization method of the $C_6H_5NH_2$ monomer. A total of 2 mL of $C_6H_5NH_2$ were reacted with 50 mL HCL and named as solution A. Furthermore, the $(NH_2)_4S_2O_8$ powder of 6.72 g was added to 50 mL H_2O and named as solution B. Solutions A and B were each stirred by using a magnetic stirrer at a speed of 650 rpm for 60 minutes and then this solution was allowed to stand for 1 hour followed by the stirring process by using magnetic stirrer for 120 minutes with a speed of 450 rpm which was then allowed to stand for 24 hours to obtain a dark green precipitate. To obtain PANI, the precipitate was then washed by using 50 mL HCL and followed by a washing process with H_2O followed by a filtering and drying process for 60 minutes at 100 °C.

2. 4. Synthesis of Fe₃O₄/AC/PANI Nanocomposites
The Fe₃O₄/AC/PANI nanocomposites were synthesized by using a simple precipitation method. A total of 3.0 g of Fe₃O₄/AC with an AC mass of 0.1 g and a mass of 0.36 g PANI were dissolved in 50 mL H₂O. The solution was then stirred by using a magnetic stirrer at 760 rpm for 15 minutes. Besides, the solution was filtered to obtained the Fe₃O₄/AC/PANI precipitate and continued with the drying process at 100 °C for 60 minutes. The process was repeated 5 times with variations in AC mass on the Fe₃O₄/AC nanocomposites of 0.1, 0.2, 0.3, 0.4, and 0.5 g. Thus, in this work, there were 6 samples, these are, Fe₃O₄ (coded AC-0), Fe₃O₄/AC/PANI nanocomposites with AC mass variations of 0.1, 0.2, 0.3, 0.4 and 0.5 g which were consecutively coded with AC-0.1, AC -0.2, AC-0.3, AC-0.4, and AC-0.5. The mechanism of formation of Fe₃O₄/AC/PANI nanocomposites carried out in this study was illustrated in Figure 1.

2. 5. Characterizations The structure of the Fe₃O₄/AC/PANI nanocomposites were characterized by using X-ray diffractometer (XRD), Cu-Kα 1.540 Å. Scanning electron microscopy (SEM)-EDAX was used to observe the morphology and composition of the Fe₃O₄/AC/PANI nanocomposites constituents. The Fe₃O₄/AC/PANI nanocomposites functional group was characterized by an FTIR spectrometer. The optical properties of the Fe₃O₄/AC/PANI nanocomposites were obtained from the characterization by using a UV-Vis spectrometer. Furthermore, radar absorption of the Fe₃O₄/AC/PANI nanocomposites was investigated by employing a vector network analyzers (VNA).

3. RESULTS AND DISCUSSION

The X-ray diffraction patterns of AC and PANI are shown in Figure 2. In Figure 2 (a), the peak of AC diffraction is identified at position 2θ around 23.6°, broad peak at 43.8° and 67.8°, where all three peaks show sequential diffraction (002), (100), and (004) corresponding to the graphite lattice [23,24]. Figure 2 (b) shows the diffraction pattern of PANI with a broad amorphous peak at position 2θ about 25.3° of the plane (200). The emergence of the broad amorphous peak shows the existence of parallel and repeated polymer chains and yields information if PANI is in the form of
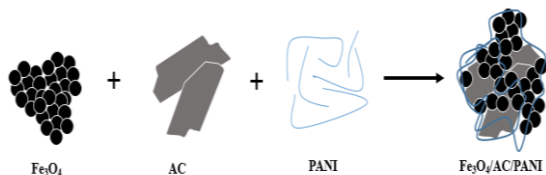
emeraldine salt [25]. Furthermore, Figure 3 indicates the results of the XRD characterization of Fe₃O₄/AC/PANI nanocomposites. Phase analysis of the nanocomposites were carried out by comparing the diffraction patterns of the characterization results with the ICSD-30860 model data, which identified several peaks at positions 2θ 30.1° (002), 35.5° (113), 43.2° (004), 47.3° (133), 53.6° (224), 57.1° (115) and 62.7° (044). These peaks confirm that the nanocomposites are only composed of one crystalline phase of Fe₃O₄. The absence of AC peak is caused by the mass of AC which tends to be small when compared to Fe₃O₄ in the composites. Meanwhile, the emergence of PANI peak is caused by this polymer having an amorphous structure. Based on the results of the phase analysis, Fe₃O₄/AC/PANI nanocomposites have an inverse cubic spinel structure with $a = b = c$ values ranging from 8.366 to 8.382 Å which correspond to the results of previous research [15].

The particle size of the Fe₃O₄/AC/PANI nanocomposites was analyzed quantitatively by using the Scherrer equation shown in Equation (1).

$$D = \frac{K.\lambda}{\beta.\cos\theta} \tag{1}$$

where D is the particle size (nm), K is a constant (0.94), λ is the wavelength (1.5443 Å), β is the full width of half-maximum, and θ is the Bragg angle from the highest peak [2]. The particle sizes obtained from the fitting results by using the Lorentzian method are shown in Table 1.
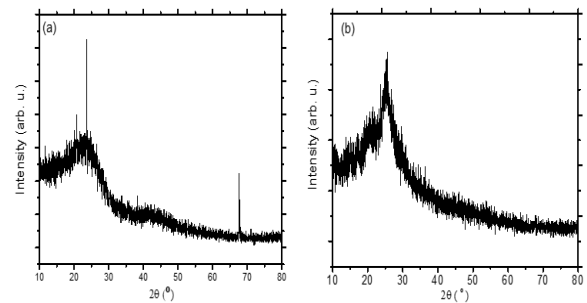

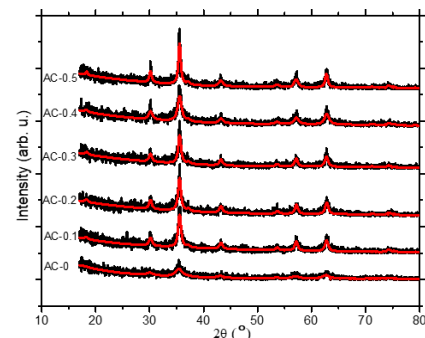**Figure 2.** X-ray diffraction patterns of (a) AC and (b) PANI

Figure 3. XRD patterns of Fe₃O₄/AC/PANI nanocomposites

Figure 1. Formation mechanism of Fe₃O₄/AC/PANI nanocomposites

TABLE 1. Particle size of Fe_3O_4/AC/PANI nanocomposites

Samples	2θ at the highest peak (°)	Particle Size (nm)
AC-0	35.4	9.87
AC-0.1	35.6	19.49
AC-0.2	35.5	21.49
AC-0.3	35.6	25.72
AC-0.4	35.5	16.90
AC-0.5	35.5	24.74

In general, the addition of the composition of AC and PANI to Fe_3O_4 nanoparticles causes the crystallinity level of Fe_3O_4 to increase. This is proven in Figure 3 which shows that the peaks of Fe_3O_4 in nanocomposites (AC-0 to AC-0.5) appear sharper when compared to pure Fe_3O_4. The increase in AC composition in Fe_3O_4/AC/PANI nanocomposites results in an increase in the intensity of the Fe_3O_4 peak except for AC-0.4 which is lower when compared to AC-0.3. This is because the AC-0.4 particle size is lower than other nanocomposites of particle sizes. This is also confirmed in Table 1 which shows the particle size of the sample.

Figure 4 portrays the FTIR spectrum of PANI, AC, Fe_3O_4 nanoparticles and Fe_3O_4/AC/PANI nanocomposites. The spectrum of the PANI sample indicates vibrational peaks at wavenumbers 825, 1184, 1336, 1504, and 1587 cm^{-1}. Meanwhile, the vibrations observed in the wavenumber of 825 cm^{-1} shows the C-H vibrations. These results seem similar to the results of previous studies that detected C-H vibrations at wavenumbers of 812 cm^{-1} [26]. The functional group of N = Q = N is detected at a wavenumber of 1184 cm^{-1}, where Q is a quinoid [27] which, at a wavenumber of 1336 cm^{-1}, is the vibration of C-N. The strongest vibrational peaks were detected at wavenumbers of 1504 and 1587 cm^{-1} which are related to the functional groups of C = C quinoids and benzoic. The intensity of transmittance in the quinoid and benzoic groups has the same value, confirming that PANI is in the form of
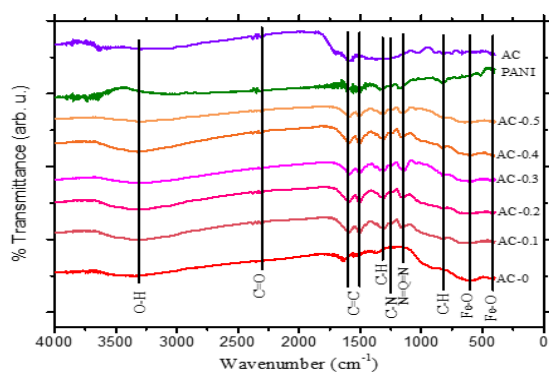
Figure 4. IR spectrum of AC-0, PANI, and AC

emeraldine salt. In addition to the 5 main vibrations from PANI, vibrations in the region from 3400 to 3500 cm^{-1} were also detected, indicating vibrations from N-H which originates from the aromatic amine functional group. This was also confirmed by previous studies that detected aromatic amine functional groups at wavenumbers of 3500 cm^{-1} [27].

Pure AC samples shown in the FTIR spectrum show vibrations from C = C, C = O, and O-H from the carboxyl group and C-O stretching derived from the acid used to activate carbon. Sequentially, these vibrations were detected at wavenumbers of 1592, 1702, 3200, and 1032 cm^{-1}. And the results correspond to the previous studies [28]. Meanwhile, the Fe_3O_4 nanoparticles depicted by AC-0 spectrum several main vibrations were detected in the form of Fe-O at a wavenumber of 418 cm^{-1} and in the region of 541-651 cm^{-1}, which sequentially showed octahedral and tetrahedral Fe-O vibrations. This confirms the XRD results stating that Fe_3O_4 has an inverse spinel cubic structure composed of octahedral and tetrahedral crystal systems. These results correspond to the previous studies that showed Fe-O vibrations at 417 cm^{-1} [29] and 580-590 cm^{-1} [30]. Interestingly, after Fe_3O_4 was composited with AC and PANI in AC-0.1 to AC-0.5 samples, it was observed that the transmittance intensity of the Fe-O functional groups decreased with the increase in AC composition. This confirms that the Fe_3O_4 mass ratio has decreased after it was compiled with AC and PANI. The visible shift of vibration peaks from PANI after being composed of Fe_3O_4 and AC nanoparticles. Vibration N = Q = N was detected at a wavenumber of 1153 cm^{-1}, C-N at a wavenumber of 1315 cm^{-1}, and C = C at a wavenumber of 1508 and 1591 cm^{-1}. Furthermore, the phenomenon of decreasing the intensity of transmittance at 3200 cm^{-1} wave number shows the O-H functional group. This happens because O-H is a carboxyl functional group with a negative charge so that when composited with positively charged Fe-O, it will bind to one another.

The SEM images of Fe_3O_4/AC/PANI nanocomposites with an AC composition of 0.3 g is shown in Figure 5. As shown in Figure 5 (a), the morphology of the nanocomposites consists of 3 particle shapes namely spheres, chunks, and worm-like structures. Sequentially, these shapes describe the Fe_3O_4 nanoparticles, AC [31,32], and PANI [33]. Qualitatively, it is observed that the sphere of Fe_3O_4 tends to agglomerate. The size of Fe_3O_4 nanoparticles is smaller than that of AC which has relatively irregular chunks. In addition, the AC surface also shows some agglomeration of Fe_3O_4, while PANI fills the gap between Fe_3O_4 and AC [27]. Illustrated in Figure 1, AC is a carbon material that is activated with acids to form OH-functional groups, so that the AC will bind to the positive charge of Fe_3O_4 which causes the Fe_3O_4 to fill the surface of the AC. Based on Figure 5(a), few AC surfaces are covered by
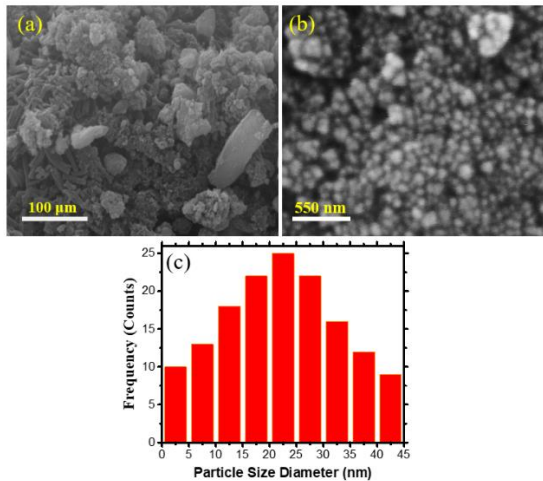
Figure 5. SEM images of AC-0.3 with (a) 5000 and (b) 200,000 magnifications, and (c) particles size distribution

agglomeration of Fe_3O_4. This is because the density of Fe_3O_4 is higher than that of AC [22]. Figure 5(b) indicates the morphology of Fe_3O_4 nanoparticles with a magnification of 200,000 magnification and shows that the Fe_3O_4 nanoparticles are evenly dispersed on the AC surface. Based on the results of data analysis in Figure 5(c), it is observed that the particle size distribution of Fe_3O_4 is 21.5 nm. This approximates the particle size values of the XRD results calculated in Table 1. Furthermore, the EDAX results show that the composition of heavy elements C, O, and Fe are 28.17, 19.63, and 52.20%, respectively, which confirms the presence of Fe_3O_4 nanoparticles, AC, and PANI that form Fe_3O_4/AC/PANI composites. The presence of Fe_3O_4 was confirmed by the presence of Fe and O elements. Meanwhile, the AC and PANI were confirmed by the presence of element C, which is carbon as the main element of AC and the benzoic and quinoid ring bonds of PANI.

The optical properties of Fe_3O_4, AC, PANI, and Fe_3O_4/AC/PANI nanocomposites with variations in AC composition were characterized by using UV-Vis at a wavelength between 350-700 nm. Figure 6 shows the UV-Vis spectrum of Fe_3O_4, PANI, and AC samples. The Fe_3O_4 nanoparticle spectrum shows absorption at a wavelength of 351 nm which shows the characteristic of Fe ions located at the octahedral site. This is in accordance with previous research stating if the absorption of Fe_3O_4 occurs in the range of 300-750 nm [34]. Qualitatively, it is observed that PANI has the highest absorption value compared to Fe_3O_4 and AC nanoparticles. Based on UV-Vis results, two absorption peaks in PANI were detected at the position of 355 and 512 nm. The peak at a wavelength of 355 nm indicates the π-π* transition, while the absorption at 512 nm indicates the π-π* transition from the benzoic ring to the quinoid ring.

The absorbance spectrum of Fe_3O_4/AC/PANI nanocomposites with variations in the AC mass composition is illustrated in Figure 7. Based on the figure, the absorption at wavelengths ranging from 510.7 nm to 514.5 nm is shown in Table 2. When compared absorption at wavenumbers around 512 nm (Figure 6) is found, the range of wave numbers shown in Figure 6 is wider with higher absorption. That is because the absorption at that wavelength is a combination of absorption by AC and PANI. Prior to being compiled with Fe_3O_4 and AC, a benzoic ring transition was detected at 512 nm, and after it was made, a transition wavelength shift occurred. Theoretically, this is due to an increase in orbital antibonding energy, which is due to the interaction between PANI and Fe_3O_4/AC. Such results were confirmed by a previous work of a shift in absorption peaks from PANI as a polymer after being combined with Fe_3O_4 nanoparticles [1].

Theoretically, electrons in the outer shell of an atom absorbing radiation energy shift to a level with higher energy or called electron excitation [35]. Thus, the absorbance of the nanocomposite is related to the energy used by electrons to move from the valence band to the conduction band (excitation) called the energy gap [36]. The direct transition of electrons written in Equation (2) was used to calculate the energy gap of the samples.
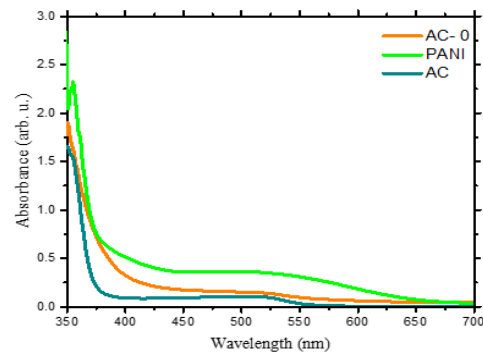
$$(\alpha h v) = A(h v - E_g)^2 \tag{2}$$
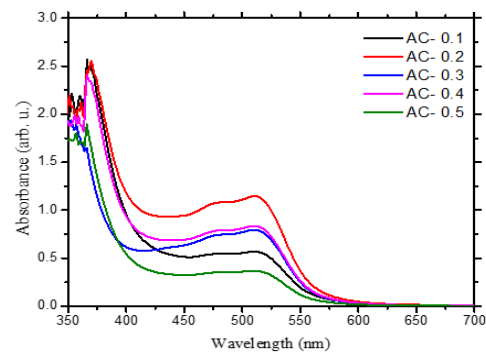

Figure 6. Absorbance of the AC-0, PANI, and AC

Figure 7. Absorbance of the Fe_3O_4/AC/PANI nanocomposites

where α is the absorption coefficient, A is the effective mass of the electron, h is the Planck constant which is 6.55×10^{-34} Js, and v is the frequency [35]. The energy gap values were analyzed by using the Tauc plot method, where the energy gap is an intercept on the x-axis of the graph of the relationship between hv and $(\alpha hv)^2$.

The results of the fitting by using the Tauc plot method to obtain the energy gap values are shown in Figure 8. The energy gap value of the Fe_3O_4 nanoparticles is shown in Figure 8 with the AC-0 code of 3.307 eV. This result is similar to a previous study that obtained an energy gap value of Fe_3O_4 of 2.87 eV [37]. In the AC and PANI materials, the energy gap values are 3.342 and 3.302 eV, respectively. These are also consistent with previous studies showing that AC has an energy gap value of less than 4.0 eV [38] and approximately 3.0 eV for PANI [39].

The energy gap of the Fe_3O_4/AC/PANI nanocomposites is shown in Table 2. The increase in the energy gap of the Fe_3O_4/AC/PANI nanocomposites is influenced by the mass of the AC, whereas the AC composition increases, the energy gap value also augment. The difference in the energy gap value between Fe_3O_4 nanoparticles and Fe_3O_4/AC/PANI nanocomposites is influenced by particle size. Based on the calculations by using Equation (1), the particle size of Fe_3O_4 nanoparticles is 9.87 nm which is smaller than the particle size of Fe_3O_4/AC/PANI nanocomposites. This causes the energy gap value of Fe_3O_4 to be greater than the nanocomposites as the effect of the particle size of the samples. Theoretically, the particle size is inversely proportional to the particle size of the material [37,40]. In addition, the energy gap value is also influenced by the absorption wavelength, where the higher the wavelength, the lower the energy gap value is. The relationship between the energy gap and absorption wavelength values in this study are shown in Table 2.

Reflection loss is a characteristic that shows the ability of radar wave absorption from Fe_3O_4/AC/PANI nanocomposites. Figure 9 shows RL of the Fe_3O_4/AC/PANI nanocomposites at a frequency of
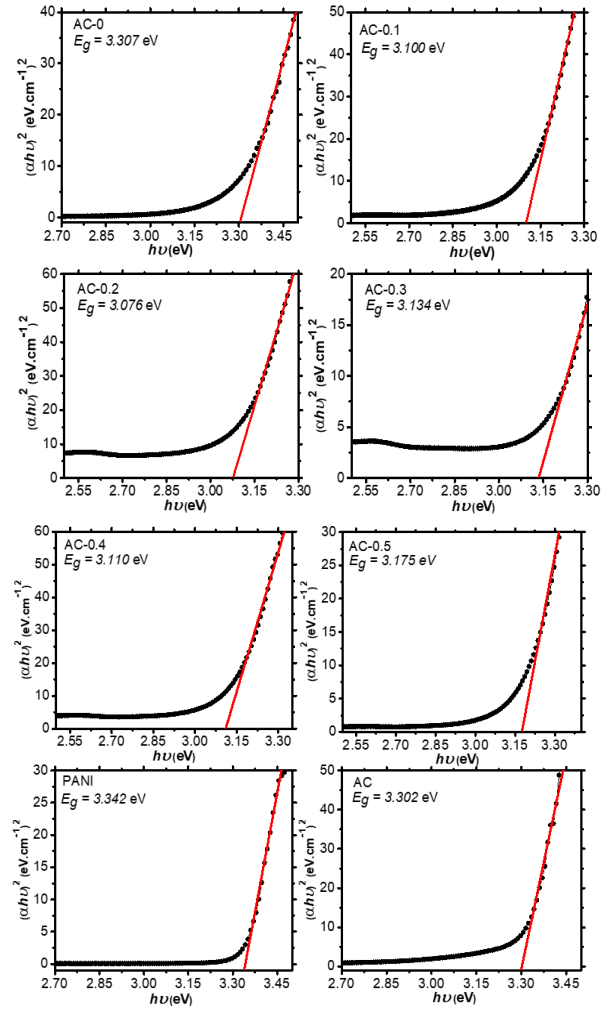

Figure 8. Energy gap of the Fe_3O_4/AC/PANI nanocomposites

8-12 GHz which were calculated by using Equations (3) and (4).

$$RL = 20\log\left|\frac{Z_{in} - Z_0}{Z_{in} + Z_0}\right| \tag{3}$$

where Z_{in} value was calculated with Equation (4):

$$Z_{in} = Z_0\sqrt{\mu_r\varepsilon_r}\tanh\left[j\frac{2\pi fd}{c}\sqrt{\mu_r\varepsilon_r}\right] \tag{4}$$

where Z_{in} and Z_{in} are input and output impedance values. While μ_r and ε_r are the permeability and complex permittivity of the material, c represents the velocity of the radar in a vacuum, f is the frequency of radar, and d is the thickness of the material when tested [41].

Fe_3O_4 has an RL of -5.58 dB at a frequency of 10.58 GHz. The low RL value owned by Fe_3O_4 is due to the fact that this sample only consists of magnetic material, thus RAM only absorbs the magnetic part of the radar. In this study, the increase in radar absorption is increased by

TABLE 2. Energy gap of the Fe_3O_4/AC/PANI nanocomposites

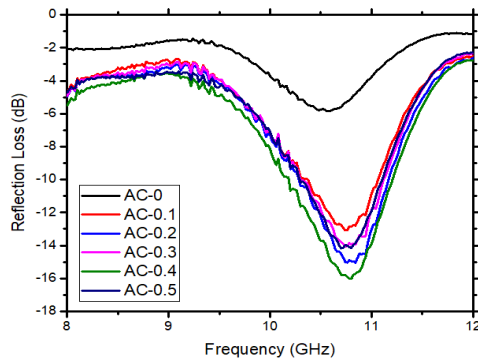| Samples	Wavelength (nm)	Energy gap (eV)
Fe_3O_4	351.0	3.307
AC-0.1	514.2	3.100
AC-0.2	514.5	3.076
AC-0.3	512.2	3.134
AC-0.4	513.2	3.110
AC-0.5	510.7	3.175
PANI	355.0	3.342
AC	510.0	3.302

Figure 9. Reflection loss of the Fe$_3$O$_4$/AC/PANI nanocomposites

compiling Fe$_3$O$_4$ with AC and PANI materials. That is because AC belongs to good dielectric material and PANI is classified as a conductive polymer. Based on Figure 9, it is noticed that the absorption capability of radar from Fe$_3$O$_4$/AC/PANI nanocomposites is stronger than that of Fe$_3$O$_4$ nanoparticles. This indicates that the absorption properties of radar increase if added by AC and PANI materials. Physically, this phenomenon occurs since the absorption of radar from Fe$_3$O$_4$ nanoparticles only comes from natural resonance and domain wall resonance, so that with the addition of PANI and AC, the dielectric loss properties of the two materials are introduced and the interface polarization between Fe$_3$O$_4$ and AC or Fe$_3$O$_4$ with PANI is introduced. In detail, the *RL* values of nanocomposites are shown in Table 3. Based on Table 3, it can be seen that the *RL* values of the Fe$_3$O$_4$/AC/PANI nanocomposites are higher than those of MWCNT/Fe$_3$O$_4$ [42] and GN-pFe$_3$O$_4$@ZnO [43]. The addition of dielectric material also causes the absorption bandwidth of the Fe$_3$O$_4$/AC/PANI nanocomposites to widen. If in Fe$_3$O$_4$ nanoparticles, the absorption bandwidth is 1.02 GHz, then when the composite bandwidth of the absorption is done, it increases within the composition of AC, which is 1.26, 1.38, 1.58, 1.68, and 1.74 GHz, respectively.

TABLE 3. *RL* value of the Fe$_3$O$_4$/AC/PANI nanocomposites

Samples	RL (dB)
AC-0	-5.58
AC-0.1	-13.09
AC-0.2	-15.00
AC-0.3	-14.06
AC-0.4	-15.80
AC-0.5	-13.99
AC@Fe$_3$O$_4$	-8.99 [22]
MWCNT/Fe$_3$O$_4$	-10.0 [42]
GN-pFe$_3$O$_4$@ZnO	<-10 [43]

Based on the results of the previous research, it was shown that, if the *RL* value obtained <-15 dB, it indicates that if 96.9% of the radar waves are absorbed by the nanocomposite. Meanwhile, if the RL value obtained <-20 dB, then the absorbed wave is almost 99.0% [44]. In this research, the RL value of nanocomposites has a range between -13 to -16 dB or <-20 dB. Thus, it can be concluded that the waves absorbed by nanocomposites in this study are around 96.9 - 99.0%. Two main aspects affecting the increase of radar absorption by Fe$_3$O$_4$/AC/PANI nanocomposites in this study are first, the efficient complementarity between dielectric loss and magnetic loss which is indicated by the relative permittivity and permeability values must be fulfilled [43,45]. If Fe$_3$O$_4$ nanoparticles stand alone as a compiler of RAM, it can be construed that the resulting *RL* value is still low. This is due to the large disparity between permeability and permittivity which interferes with impedance matching. Thus, in the Fe$_3$O$_4$/AC/PANI system, the Fe$_3$O$_4$ nanoparticles act as absorbents of the magnetic parts, and PANI, as well as AC, are as dielectric absorbers of incoming radar. Besides, the AC also acts as a nucleation site for Fe$_3$O$_4$ which prevents or reduces the aggregation of these nanoparticles. Second, there is interfacial polarization between Fe$_3$O$_4$-AC or between Fe$_3$O$_4$-PANI, where multi-interfaces on nanocomposites will produce significant polarization interfaces that will increase the value of dielectric loss at high frequencies [41]. This is indicated when the addition of AC and PANI absorption material occurs at a frequency of around 11 GHz. Thus, the development of Fe$_3$O$_4$/AC/PANI nanocomposites in this research provides new opportunities for large-scale development for the application of high-performance microwave absorbing materials based on local natural materials through environmentally friendly synthesis.

4. CONCLUSION

The Fe$_3$O$_4$/AC/PANI nanocomposites were successfully synthesized by using an environmental precipitation method. The presence of Fe$_3$O$_4$ is detected as crystalline with a cubic structure. Meanwhile, the presence of AC and PANI is confirmed by C-C bond, COOH vibrations, benzoic ring vibration, and quinonoid bond. AC acts as a nucleation site for Fe$_3$O$_4$ and PANI acts as a connector. The energy gap of Fe$_3$O$_4$/AC/PANI nanocomposites ranges from 3.000 to 3.175 eV. With the addition of AC and PANI in the Fe$_3$O$_4$/AC/PANI nanocomposites, their *RL* increases significantly because the nanocomposites consist of magnetic loss and dielectric loss which increases the radar absorption. Interestingly, the *RL* value of the Fe$_3$O$_4$/AC/PANI nanocomposites ranges from -13.0 to -15.8 dB which shows their radar absorption capability is in the range of 96.9% - 99.0%.

5. ACKNOWLEDGMENT

6. REFERENCES

1. Cui, C., Du, Y., Li, T., Zheng, X., Wang, X., Han, X. and Xu, P., "Synthesis of electromagnetic functionalized Fe_3O_4 microspheres/polyaniline composites by two-step oxidative polymerization", *The Journal of Physical Chemistry B*, Vol. 116, (2012), 9523–9531.

2. Taufiq, A., Bahtiar, S., Sunaryono., Hidayat, N., Hidayat, A., Mufti, N., Diantoro, M., Fuad, A., Munasir., Rahmawati, R., Adi, W. A., Pratapa, S., and Darminto., "Preparation of superparamagnetic $Zn_{0.5}Mn_{0.5}Fe_2O_4$ particle by coprecipitation-sonochemical method for radar absorbing material", *IOP Conference Series: Materials Science and Engineering*, Vol. 202, (2017), 012024.

3. Salimkhani, H., Movassagh-Alanagh, F., Aghajani, H. and Osouli-Bostanabad, K., "Study on the magnetic and microwave properties of electrophoretically deposited nano-Fe_3O_4 on carbon fiber", *Procedia Materials Science*, Vol. 11, (2015), 231–237.

4. Bhattacharya, P., Sahoo, S. and Das, C. K., "Microwave absorption behavior of MWCNT based nanocomposites in X-band region", *Express Polym Lett*, Vol. 7, (2013), 212–223.

5. Li, W., Lin, L., Li, C., Wang, Y. and Zhang, J., "Radar absorbing combinatorial metamaterial based on silicon carbide/carbon foam material embedded with split square ring metal", *Results in Physics*, Vol. 12, (2019) 278–286.

6. Wang, C., Chen, M., Lei, H., Yao, K., Li, H., Wen, W. and Fang, D., "Radar stealth and mechanical properties of a broadband radar absorbing structure", *Composites Part B: Engineering*, Vol. 123, (2017), 19–27.

7. Bhattacharya, P., Sahoo, S. and Das, C. K., "Microwave absorption behavior of MWCNT based nanocomposites in X-band region", *Express Polymer Letters*, Vol. 7, (2013), 212–223.

8. Xia, R., Yin, Y., Zeng, M., Dong, H., Yang, H., Zeng, X., Tang, W. and Yu, R., "High-Frequency absorption of the hybrid composites with spindle-like Fe_3O_4 nanoparticles and multiwalled carbon nanotubes", *Nano*, Vol. 11, (2016), 1650097.

9. Wei, S., Yan, R., Shi, B. and Chen, X., "Characterization of flexible radar-absorbing materials based on ferromagnetic nickel micron-fibers", *Journal of Industrial Textiles*, Vol. 49, (2018), 58-70.

10. Rahmawati, R., Melati, A., Taufiq, A., Sunaryono., Diantoro, M., Yuliarto, B., Suyatman, S., Nugraha, N. and Kurniadi, D., "Preparation of MWCNT-Fe_3O_4 nanocomposites from iron sand using sonochemical route", *IOP Conference Series: Materials Science and Engineering*, Vol. 202, (2017), 012013.

11. Bagheripour, E., Moghadassi, A. R. and Hosseini, S. M., "Incorporated polyacrylic acid-co-Fe_3O_4 nanoparticles mixed matrix polyethersulfone based nanofiltration membrane in desalination process". *International Journal of Engineering (IJE), IJE TRANSACTIONS C: Aspects*, Vol. 30, No. 6, (2017), 821-829.

12. Taufiq, A., Saputro, R. E., Sunaryono., Hidayat, N., Hidayat, A., Mufti, N., Diantoro, M., Patriati, A., Mujamilah., Putra, E. G. R. and Nur, H., "Fabrication of magnetite nanoparticles dispersed in olive oil and their structural and magnetic investigations", *IOP Conference Series: Materials Science and Engineering*, Vol. 202, (2017), 012008.

13. Panwar, R., Puthucheri, S., Agarwala, V. and Singh, D., "Effect of particle size on radar wave absorption of fractal frequency selective surface loaded multilayered structures", *IEEE*, Vol. 12, (2014), 186–189.

14. Mingdong, C., Huangzhong, Y., Xiaohua, J. and Yigang, L., "Optimization on microwave absorbing properties of carbon nanotubes and magnetic oxide composite materials", *Applied Surface Science*, Vol. 434, (2018), 1321–1326.

15. Kumar, S. and Jain, S., "One-step synthesis of superparamagnetic Fe_3O_4@PANI nanocomposites", *Journal of Chemistry*, Vol. 2014, (2014), 1–6.

16. Liu, P., Huang, Y., Yang, Y., Yan, J. and Zhang, X., "Sandwich structures of graphene@Fe_3O_4@PANI decorated with TiO_2 nanosheets for enhanced electromagnetic wave absorption properties", *Journal of Alloys and Compounds*, Vol. 662, (2016), 63–8.

17. Zhu, Y-F., Ni, Q-Q., Fu, Y-Q. and Natsuki, T., "Synthesis and microwave absorption properties of electromagnetic functionalized Fe_3O_4–polyaniline hollow sphere nanocomposites produced by electrostatic self-assembly", *Journal of Nanoparticle Research*, Vol. 15, (2013).

18. Djilani, C., Zaghdoudi, R., Djazi, F., Bouchekima, B., Lallam, A., Modarressi, A. and Rogalski, M., "Adsorption of dyes on activated carbon prepared from apricot stones and commercial activated carbon" *Journal of the Taiwan Institute of Chemical Engineers*, Vol. 53, (2015), 112–121.

19. Islam, MdA., Sabar, S., Benhouria, A., Khanday, W. A., Asif, M. and Hameed, B. H., "Nanoporous activated carbon prepared from karanj (Pongamia pinnata) fruit hulls for methylene blue adsorption", *Journal of the Taiwan Institute of Chemical Engineers*, Vol. 74, (2017), 96–104.

20. Masomi, M., Ghoreyshi, A. A., Najafpour, G. D. and Mohamed, A. R. B., "Adsorption of phenolic compounds onto the activated carbon synthesized from pulp and paper mill sludge: equilibrium isotherm, kinetics, thermodynamics and mechanism studies", *International Journal of Engineering (IJE), IJE TRANSACTIONS A: Basics*, Vol. 27, No. 10, (2014), 1485-1494.

21. Huang, Y-P., Hou, C-H., His, H-C. and Wu, J-W., "Optimization of highly microporous activated carbon preparation from Moso bamboo using central composite design approach", *Journal of the Taiwan Institute of Chemical Engineers*, Vol. 50, (2015), 266–275.

22. Yin, P., Deng, Y., Zhang, L., Li, N., Feng, X., Wang, J. and Zhang, Y., "Facile synthesis and microwave absorption investigation of activated carbon@Fe_3O_4 composites in the low-frequency band", *RSC Advances*, Vol. 8, (2018), 23048–23057.

23. Mopoung, S., Moonsri, P., Palas, W. and Khumpai, S., "Characterization and properties of activated carbon prepared from tamarind seeds by KOH activation for Fe(III) adsorption from aqueous solution", *The Scientific World Journal*, Vol. 2015, (2015), 1–9.

24. Drewniak, S., Muzyka, R., Stolarczyk, A., Pustelny, T., Kotyczka-Morańska, M. and Setkiewicz, M., "Studies of reduced graphene oxide and graphite oxide in the aspect of their possible application in gas sensors", *Sensors*, Vol. 16, (2016), 103.

25. Li, L., Qin, Z-Y., Liang, X., Fan, Q-Q., Lu, Y-Q., Wu, W-H. and Zhu, M. F., "Facile fabrication of uniform core−shell structured carbon nanotube−polyaniline nanocomposites", *The Journal of Physical Chemistry C*, Vol. 113, (2009), 5502–5507.

26. Prasanna, B. P., Avadhani, D. N., Chaitra, K., Nagaraju, N. and Kathyayini, N., "Synthesis of polyaniline/MWCNTs by interfacial polymerization for superior hybrid super capacitance performance", *Journal of Polymer Research*, Vol. 25, (2018), 123.

27.   Olad, A. and Gharekhani, H., "Study on the capacitive performance of polyaniline/activated carbon nanocomposite for supercapacitor application", *Journal of Polymer Research*, Vol. 23, (2016), 147.

28.   Hashemi, S. Y., Mousavi, S.A., Aghaali, E., Kamarehie, B. and Jafari, A., "Nitrate removal from aqueous solutions using granular activated carbon modified with iron nanoparticles", *International Journal of Engineering (IJE), IJE TRANSACTIONS A: Basics*, Vol. 31, No. 4, (2018), 554-563.

29.   Wang, B., Wang, B., Wei, P., Wang, X. and Lou, W., "Controlled synthesis and size-dependent thermal conductivity of Fe_3O_4 magnetic nanofluids", *Dalton Trans*, Vol. 41, (2012), 896–899.

30.   Yusoff, A. H. M., Salimi, M.N. and Jamlos, M.F., "Synthesis and characterization of biocompatible Fe_3O_4 nanoparticles at different pH", *AIP Conference Proceedings*, Vol. 1835, (2017), 020010.

31.   Kakavandi, B., Jonidi, A., Rezaei, R., Nasseri, S., Ameri, A. and Esrafily, A., "Synthesis and properties of Fe_3O_4-activated carbon magnetic nanoparticles for removal of aniline from aqueous solution: equilibrium, kinetic and thermodynamic studies", *Iranian Journal of Environmental Health Science & Engineering*, Vol. 10, (2013), 19.

32.   Juang, R-S., Yei, Y-C., Liao, C-S., Lin, K-S., Lu, H-C, Wang, S-F. and Sun, A-C., "Synthesis of magnetic Fe_3O_4/activated carbon nanocomposites with high surface area as recoverable adsorbents", *Journal of the Taiwan Institute of Chemical Engineers*, Vol. 90, (2018), 51–60.

33.   Butoi, B., Groza, A., Dinca, P., Balan, A. and Barna, V., "Morphological and structural analysis of polyaniline and poly(o-anisidine) layers generated in a DC glow discharge plasma by using an oblique angle electrode deposition configuration", *Polymers*, Vol. 9, (2017), 732.

34.   Feng, X., Guo, H., Patel, K., Zhou, H. and Lou, X., "High performance, recoverable Fe_3O_4/ZnO nanoparticles for enhanced photocatalytic degradation of phenol", *Chemical Engineering Journal*, Vol. 244, (2014), 327–334.

35.   Rahman, M. M., Hussain, M. M. and Asiri, A. M., "Fabrication of 3-methoxy phenol sensor based on Fe_3O_4 decorated carbon nanotube nanocomposites for environmental safety: Real sample analyses", *PLOS ONE*, Vol. 12, (2017), e0177817.

36.   Suprayogi, T., Masrul M. Z., Diantoro, M., Taufiq, A., Fuad, A. and Hidayat, A., "The effect of annealing temperature of ZnO compact layer and TiO_2 mesoporous on photo-supercapacitor performance", IOP Conference Series: Materials Science and Engineering, Vol. 515, (2019), 012006.

37.   El Ghandoor, H., Zidan, H.M., Khalil, M. M. and Ismail, M. I. M., "Synthesis and some physical properties of magnetite (Fe_3O_4) nanoparticles", *Int J Electrochem Sci*, Vol. 7, (2012), 5734–5745.

38.   Bagheri. S., Muhd Julkapli, N. and Bee Abd Hamid S., "Functionalized activated carbon derived from biomass for photocatalysis applications perspective", *International Journal of Photoenergy*, Vol. 2015, (2015), 1–30.

39.   Almasi, M. J., Fanaei Sheikholeslami, T. and Naghdi M.R., "Bandgap study of polyaniline and polyaniline/MWNT nanocomposites with in situ polymerization method", *Composites Part B: Engineering*, Vol. 96, (2016), 63–68.

40.   Bagbi, Y., Sarswat, A., Mohan, D., Pandey, A. and Solanki, P. R., "Lead (Pb^{2+}) adsorption by monodispersed magnetite nanoparticles: Surface analysis and effects of solution chemistry", *Journal of Environmental Chemical Engineering*, Vol. 4, (2016), 4237–4247.

41.   Yin, P., Deng, Y., Zhang, L., Huang, J., Li, H., Li, Y., Qi, Y. and Tao, Y., "The microwave absorbing properties of ZnO/Fe_3O_4/paraffin composites in low-frequency band", *Materials Research Express*, Vol. 5, No. 2, (2018), 026109.

42.   Wang, Z., Wu, L., Zhou, J., Jiang, Z. and Shen, B., "Chemoselectivity-induced multiple interfaces in $MWCNT/Fe_3O_4@ZnO$ heterotrimers for whole X-band microwave absorption", *Nanoscale*, Vol. 6, (2014), 12298–12302.

43.   Sun, D., Zou, Q., Wang, Y., Wang, Y., Jiang, W. and Li, F., "Controllable synthesis of porous $Fe_3O_4@ZnO$ sphere decorated graphene for extraordinary electromagnetic wave absorption", *Nanoscale*, Vol. 6, (2014), 6557–6562.

44.   Idris, Fmohd., Hashim, M., Abbas, Z., Ismail, I., Nazlan, R. and Ibrahim, I. R., "Recent developments of smart electromagnetic absorbers based polymer-composites at gigahertz frequencies", *Journal of Magnetism and Magnetic Materials*, Vol. 405, (2016), 197–208.

45.   Jian, X., Wu, B., Wei, Y., Dou, S. X., Wang, X., He, W. and Mahmood, N., "Facile synthesis of Fe_3O_4/GCs composites and their enhanced microwave absorption properties", *ACS Applied Materials & Interfaces*, Vol. 8, (2016), 6101–6109.

Radar Absorption Performance of Fe₃O₄/AC/PANI Nanocomposites Prepared from Natural Iron Sand

A. Taufiqᵃ, R. Sutiamiᵃ, S. U. I. Subadraᵃ, A. Hidayatᵃ, M. Diantoroᵃ, S. Sunaryonoᵃ, N. Hidayatᵃ, W. A. Adiᵇ

ᵃ Department of Physics, Faculty of Mathematics and Natural Sciences, Universitas Negeri Malang, Indonesia
ᵇ Centre for Technology of Nuclear Industry Materials, National Nuclear Energy Agency, Tangerang, Indonesia

چکیده

در این کار ، نانوذرات Fe₃O₄ از شن آهن طبیعی با کربن فعال (AC) و پلی انیلین (PANI) ترکیب شدند تا نانوکامپوزیت های Fe₃O₄ / AC / PANI با تغییرات انبوه AC از ۰/۱، ۰/۲ ، ۰/۳ ، ۰/۴ و ۰/۵ g بدست آید. فاز کریستالی نانوکامپوزیت Fe₃O₄ / AC / PANI از Fe₃O₄ با PANI دارای فاز آمورف بوده است. در همین حال ، فاز کریستالی ACبه دلیل ترکیب بسیار کم آن بی همتا بود. حضور AC از طریق ارتعاشات از گروههای عملکردی C-C و COOH مشاهده شد. وجود PANI با ارتعاشات حلقه بنزوئی و پیوندهای کوینوئید نشان داده شد. علاوه بر این ، حضور Fe₃O₄ با حضور گروههای عملکردی Fe-O از موقعیتهای هشت ضلعی و چهار ضلعی تأیید گردید. خواص نوری نانوکامپوزیت های Fe₃O₄ / AC / PANI با افزایش شکاف انرژی به همراه کاهش طول موج جذب نشان داده شد. جالب توجه است ، افزایش ترکیب AC باعث شده است که پهنای باند جذب نانوکامپوزیت های Fe₃O₄ / AC / PANI گسترده تر شود ، به طوری که جذب رادار نیز باعث کاهش مارک با از دست دادن بازتاب بیشتر است که به به -۱۵/۸ دسی بل رسیده است. افزایش عملکرد جذب رادار نانوکامپوزیت های Fe₃O₄ / AC / PANI از مکمل کارآمد بین از دست دادن دی الکتریک و ریزش مغناطیسی و قطبش بین سطحی بین Fe₃O₄-AC یا بین Fe₃O4-PANI حاصل شد.

doi: 10.5829/ije.2020.33.02b.15